Title: Calculating individual lifetime effective risk from initial mean glandular dose arising from the first screening mammogram

Abstract

Objectives: To use the initial mean glandular dose (MGD) arising from the first screening mammogram to estimate the individual total screening lifetime effective risk.

Methods: Organ doses from FFDM screening exposures (craniocaudal and mediolateral oblique for each breast) were measured using a simulated approach, with average breast thickness and adult ATOM phantoms, on 16 FFDM machines. Doses were measured using TLDs accommodated inside the ATOM phantom; examined breast MGD was calculated. Total effective risk during a client's lifetime was calculated for 150 screening scenarios of different screening commencement ages and frequencies. For each scenario, a set of conversion factors were obtained to convert MGD values into total effective risk.

Results: For the 16 FFDM machines, MGD contributes approximately 98% of total effective risk. This contribution is approximately constant for different screening regimes of different screening commencement ages. MGD contribution remains constant but the risk reduced because the radio-sensitivity of all body tissues, including breast tissue, reduces with age. Three sets of conversion factors were obtained for three screening frequencies (annual, biennial, triennial). Three relationship graphs between screening commencement age and total effective risk, as percentages of MGD, were created.

Conclusions: Graphical representation of total risk could be an easy way to illustrate the total effective risk during a client's lifetime. Screening frequency, commencement age, and MGD are good predictors for total effective risk generating more understandable data by clients than MGD.

Keywords

radiation hazards, breast dose, mammography, screening

Introduction

Breast radiation dose arising from mammography has reduced from approximately 150 mGy for film to <2 mGy for full field digital mammography (FFDM) [1]. Incident radiation exposure (Roentgens) at the breast surface and entrance surface dose (ESD) were the early quantities used to determine the radiation risk from mammography [2]. Since mammography uses low energy X-ray photons, the radiation dose inside the breast rapidly reduces as the depth increases [3]. Accordingly, different quantities have been suggested as measures for mammographic radiation risk, these include midline breast dose and total breast energy [2]. In 1976, work by Karlsson, Nygren, Wickman, and Hettinger [4] proposed the use of breast glandular tissue radiation dose as

a measure for mammographic radiation risk. By 1987, the ICRP recommended mean glandular dose (MGD) as the measure for breast dosimetry [2].

MGD is fundamentally related to target/filter combination (radiation spectrum), X-ray tube output (kV, mA, and time), breast density (glandularity) and breast size (compressed breast thickness) [3, 5, 6]. Direct estimation of MGD is difficult and it has to be calculated from multiplying the incident air kerma by conversion factors that are obtained from Monte Carlo mathematical simulations [7]. The main limitation of MGD calculations using conversion factors is that during the Monte Carlo simulations a homogenous breast phantom, ~~comprising~~ comprised of a uniform distribution of glandular tissue within fatty tissue, of different breast densities was used. As concluded by Sechopoulos et al. [8], the use of this homogenous phantom results in significant MGD overestimation. The highest MGD overestimation values were recorded at low photon energies; overestimation decreases as the photon energy increases. Sechopoulos's work agrees with that of Dance et al. [9], who reported that the use of conversion factors may result in as much as a 43% difference in calculated MGD due to glandular tissue spatial distribution. Accordingly, Geeraert et al. [10] calculated MGD for six breast phantoms with different glandular tissue distributions and different MGD values were subsequently recorded for the phantoms. Geeraert et al. [10] suggested the use of total energy imparted in glandular tissue (GIE) instead of MGD.

Mammographic radiation dose to organs *other than* the examined breast is usually assessed by the use of Monte Carlo software with mathematical heterogeneous human body phantoms. Within these phantoms, body tissues and organs are mathematically described to consider their shape, size and location. Radiation doses are calculated by determining the average radiation energy imparted to each organ.

Sechopoulos et al. [11] utilised the Geant4 Monte Carlo toolkit to simulate four-view film-screen mammography. Sechopoulos et al. estimated the radiation dose to all body tissues other than breast. They concluded that the doses were extremely small and that the Rh/Rh target/filter combination resulted in higher organ doses than those from Mo/Mo and Mo/Rh target/filter combinations. They also found that the second and third highest radiation dose, after the examined breast, was received by the pectoral muscle and contralateral breast, respectively [11]. Sechopoulos and Hendrick [12] estimated the radiation dose received by the thyroid gland during mammography. They considered the thyroid dose to be negligible in regard to radiation-induced cancer because four-view mammography would result in 1 thyroid cancer case per 166 million women imaged. Sechopoulos and Hendrick [12] also argued that the use of a thyroid shield may result in discomfort to women and interfere with positioning which may cause image artifacts. Leidens et al. [13] used the Monte Carlo PENELOPE toolkit to estimate lung, heart and red bone marrow radiation dose during standard cranio-caudal (CC) mammography with film-screen systems. They reported that only the lung received a considerable radiation dose (0.14% of the examined breast dose), while doses to the heart (0.033%) and bone marrow (0.0013%) were negligible [13].

A study by Whelan et al. [14] used thermo-luminescent dosimeters (TLDs) to measure radiation dose received by women's skin overlying the thyroid during standard 4 view screening mammography and diagnostic mammography. This study concluded that the average measured thyroid dose, which was 0.04 mGy, was insignificant compared to the 4 mGy dose received by the breast. Hatziioannou et al. [15] also utilised TLDs accommodated inside an upper body anthropomorphic Lucite phantom, comprised of Perspex slices designed to simulate female body contour. This was performed to investigate the *in vivo* measurement of dose to the breast, sternum red bone marrow (SRBM), thyroid, liver, lung, stomach, and oesophagus during 4 view screening mammography using a Giotto mammography machine (Mo/Mo target/filter). They found that breast dose contributes over 98% of the overall effective dose. SRBM and thyroid receive a radiation dose between 0.4-1.27 and 0.05-0.17 μGy/mAs, respectively, and the other organ doses were negligible [15]. The main limitations of Hatziioannou's study were that the simulated mammographic positions were CC and ML (90^{o} angle) for each breast, and the homogenous Lucite phantom was not a good simulator of the different body tissues.

Overall, there is a growing need for obtaining an easy and accurate way to determine the risk of radiation-induced cancer from screening mammography. This is particularly useful for screening justification and risk-benefit evaluation. Total effective risk during female lifetime is the recommended quantity reported by M.Ali et al. [16, 17]. Since the breast tissue receives the highest radiation dose, MGD from initial mammogram can be considered to accommodate variations amongst different FFDM machines. However, M.Ali et al. [16] have not considered MGD variations in their published mathematical model. Accordingly, this work aims to refine M.Ali et.al's model by deriving a woman's total effective risk from MGD from the initial mammogram in addition to screening commencement age and frequency.

Materials and Methods

Sixteen UK National Health Service Breast Screening Programme (NHSBSP) FFDM machines were included in this study. Machine quality control met NHSBSP standards (beam alignment, detector performance, automatic exposure control (AEC), image display monitors, image display printers, image quality, and radiation dose) [18]. Machines included 4 manufacturers: 5 Hologic (3 Selenia, 2 Selenia Dimensions), 8 GE (Seno Essential), 2 ~~machines~~ Siemens (Mammomat Inspiration) and 1 Giotto. Automatic exposure control is used to expose a PMMA-Polyethylene breast phantom on each machine.

Incident air kerma for the PMMA-Polyethylene phantom was multiplied by Dance's conversion factors [7] to obtain MGD for each machine. To replicate the compressed breast thickness and shape accurately, two breast phantoms were utilised. A semicircular phantom (95 mm diameter) with 32.5 mm thick PMMA and 20.5 mm thick polyethylene was used to simulate compressed breast in CC projection. A 150 mm X 100 mm rectangular phantom (32.5 mm thick PMMA and 25.5 mm thick polyethylene) was utilised to simulate the compressed breast in MLO projection.

Small (0.125 X 0.125 X 0.035 inches) tissue equivalent (atomic number for TLDs = 8.04 compared to that of soft tissue = 7.42) TLDs were placed inside an adult anthropomorphic ATOM dosimetry phantom [19] to measure organ dose. Absorbed radiation dose for organs was calculated by averaging the TLD values within each organ. The numbers of TLDs used for each organ are listed in Table (1), the number is consistent with other researchers [20].

Table (1) Number of TLDs utilised for organ dose measurements (n=280).

Organ	No. of TLDs	Organ	No. of TLDs
Adrenal	2	Pancreas	5
Brain	11	Pelvis BM*	17
Clavicle BM*	4	Ribs BM*	18
Cranium BM*	4	Salivary glands	6
Cervical spine BM*	2	Scapulae BM*	16
Gall bladder	5	Spleen	12
Heart	2	Sternum BM*	4
Intestine	16	Stomach	14
Kidneys	16	Thoraco-lumbar spine BM*	8
Liver	29	Thymus	4
Lungs	36	Thyroid	6
Mandible BM*	6	Urinary Bladder (UB)	13
Oesophagus	3	Uterus	3
Ovaries	2	Contralateral breast (8 for each side)	16
**BM = bone marrow.*			

Effective risk was calculated for females aged 25-75 years, the earliest and the latest possible ages of screening mammography, using Brenner's equation [21].

$$R=\sum r_T H_T$$

Where R is the effective risk, r_T is the lifetime attributable risk (LAR) of radiation-induced cancer for tissue T per unit equivalent dose to that tissue, and H_T is the equivalent dose received by tissue T.

The lifetime attributable cancer risk of different tissues (r_T) were taken from BEIR VII – Phase 2 report of National Academy of Sciences (NAS) [22]. Since these values are only presented for each decade of female age, they were plotted graphically against age in order to extrapolate an approximate value for each year of female life using a linear relationship between decades. Finally, total effective lifetime risk, during female lifetime, for different screening

commencement ages (25-~~74~~ 75 years) and for three different screening frequencies (annual, biennial, and triennial) were calculated, using the method described by M.Ali et al. [16].

Since all other body tissue doses are responsible for only 2% and the examined breast radiation dose is responsible for approximately 98% of the radiation risk, the relationship between MGD and total effective risk for each scenario was established using the data from the 16 FFDM machines to accommodate the effect of MGD variations between different FFDM on a woman's total effective risk. Relationship graphs, between screening commencement age and total effective risk, were then modified to demonstrate the relationship between screening commencement age and the MGD conversion factor for total effective risk.

Results

For the sixteen machines, the examined breast received the highest radiation dose, where total MGD from one screening visit (for both CC and MLO projections) ranged between 1.678 mGy and 2.806 mGy with a mean (95% confidence interval (CI)) of 2.019 (1.871-2.166) mGy (Table 2)**.** All machines showed MLO MGD to be higher than CC. However, MGD variation between MLO and CC differed amongst the 16 machines.

Table (2) Examined breast MGD for the sixteen FFDM machines.

Machine number	MGD (mGy)		Total MGD (mGy)
	CC view	MLO view	
1	1.160	1.271	2.431
2	1.050	1.273	2.323
3	0.843	1.164	2.007
4	0.811	1.082	1.893
5	0.927	1.082	2.009
6	0.825	0.949	1.774
7	1.169	1.637	2.806
8	0.983	1.219	2.202
9	0.854	0.977	1.831
10	1.060	1.071	2.131
11	0.825	0.853	1.678
12	0.921	1.055	1.976
13	0.918	0.941	1.859
14	0.930	0.961	1.891
15	0.787	0.969	1.756
16	0.771	0.959	1.730
Mean (95% CI)	0.927 (0.865-0.989)	1.091 (0.998-1.185)	2.019 (1.871-2.166)

In general, the three highest organ doses, after the examined breast, are the contralateral breast, sternum red bone marrow and thyroid, in descending order, respectively. The organs which received an average radiation dose of ≥0.1 μGy are presented in Table (3) as a percentage of the MGD.

Table (3) Mean organ doses for the sixteen FFDM machines (4 projections) along with their percentages in relation to the average examined breast MGD.

Organ	Radiation dose, mean (SD), μGy	Organ dose percentages of MGD, mean (SD)
Brain	0.91 (1.21)	0.05 (0.07)
Salivary	2.79 (0.93)	0.14 (0.05)
Thyroid	9.45 (3.05)	0.47 (0.13)
Oesophagus	0.26 (0.21)	0.01 (0.01)
Thymus	2.43 (1.23)	0.12 (0.06)
Heart	0.39 (0.23)	0.02 (0.01)
Lung	3.06 (1.06)	0.15 (0.05)
Liver	0.69 (0.29)	0.03 (0.01)
Gall bladder	0.19 (0.16)	0.01 (0.01)
Adrenals	0.10 (0.14)	0.01 (0.01)
Stomach	0.42 (0.21)	0.02 (0.01)
Cranium (BM)	1.56 (1.39)	0.08 (0.08)
Mandible (BM)	2.79 (0.93)	0.14 (0.05)
Cervical spine (BM)	0.30 (0.34)	0.02 (0.02)
Clavicles (BM)	9.25 (5.25)	0.45 (0.24)
Scapulae (BM)	0.17 (0.14)	0.01 (0.008)
Sternum (BM)	19.07 (6.12)	0.942 (0.25)
Ribs (BM)	3.57 (1.31)	0.18 (0.05)
Contralateral breast	28.75 (8.54)	1.42 (0.35)
Examined breast (MGD)	2018.50 (300.33)	100.00

If organ radiation doses resulting from screening mammography are considered to be constant during a female's lifetime, the changes in effective risk during a female's lifetime are only dependent on LAR reduction with age (Table 4).

Table (4) Mean calculated effective risk values for the sixteen FFDM machines for each year of female life with 95% CI.

Age (year)	Effective lifetime risk (case/10^6)		Age (year)	Effective lifetime risk (case/10^6)	
	Mean	95% CI		Mean	95% CI
25	70.00	64.88 - 75.12	51	14.10	13.07 - 15.13
26	66.38	61.53 - 71.24	52	12.93	11.99 - 13.88
27	62.77	58.18 - 67.36	53	11.82	10.96 - 12.69
28	59.16	54.83 - 63.48	54	10.76	9.98 - 11.55
29	55.54	51.48 - 59.60	55	9.76	9.04 - 10.47
30	51.93	48.13 - 55.72	56	8.81	8.16 - 9.45
31	48.59	45.04 - 52.15	57	7.91	7.33 - 8.49
32	46.36	42.97 - 49.75	58	7.06	6.54 - 7.58
33	44.18	40.95 - 47.41	59	6.27	5.81 - 6.73
34	42.06	38.98 - 45.13	60	5.53	5.12 - 5.93
35	39.99	37.06 - 42.91	61	4.84	4.49 - 5.20
36	37.97	35.19 - 40.74	62	4.21	3.90 - 4.52
37	36.00	33.37 - 38.63	63	3.63	3.36 - 3.89
38	34.09	31.60 - 36.58	64	3.10	2.87 - 3.33
39	32.23	29.88 - 34.59	65	2.63	2.44 - 2.82
40	30.43	28.20 - 32.65	66	2.21	2.05 - 2.37
41	28.68	26.58 - 30.78	67	1.84	1.71 - 1.98
42	26.98	25.01 - 28.95	68	1.53	1.41 - 1.64
43	25.34	23.48 - 27.19	69	1.27	1.17 - 1.36
44	23.75	22.01 - 25.48	70	1.06	0.98 - 1.14
45	22.21	20.58 - 23.83	71	0.90	0.84 - 0.97
46	20.72	19.21 - 22.24	72	0.80	0.74 - 0.86
47	19.29	17.88 - 20.70	73	0.75	0.70 - 0.81
48	17.91	16.60 - 19.22	74	0.75	0.70 - 0.81
49	16.59	15.38 - 17.80	75	0.75	0.69 - 0.80
50	15.32	14.20 - 16.44			

The graphical presentation of the relationship between screening commencement age (X-axis) and average total effective risk (Y-axis) for the sixteen FFDM machines is demonstrated in Figure (1).

This was based on the method described by M.Ali et al. [16]. In this figure the cessation age of screening mammography is set at a constant level (75 years old).

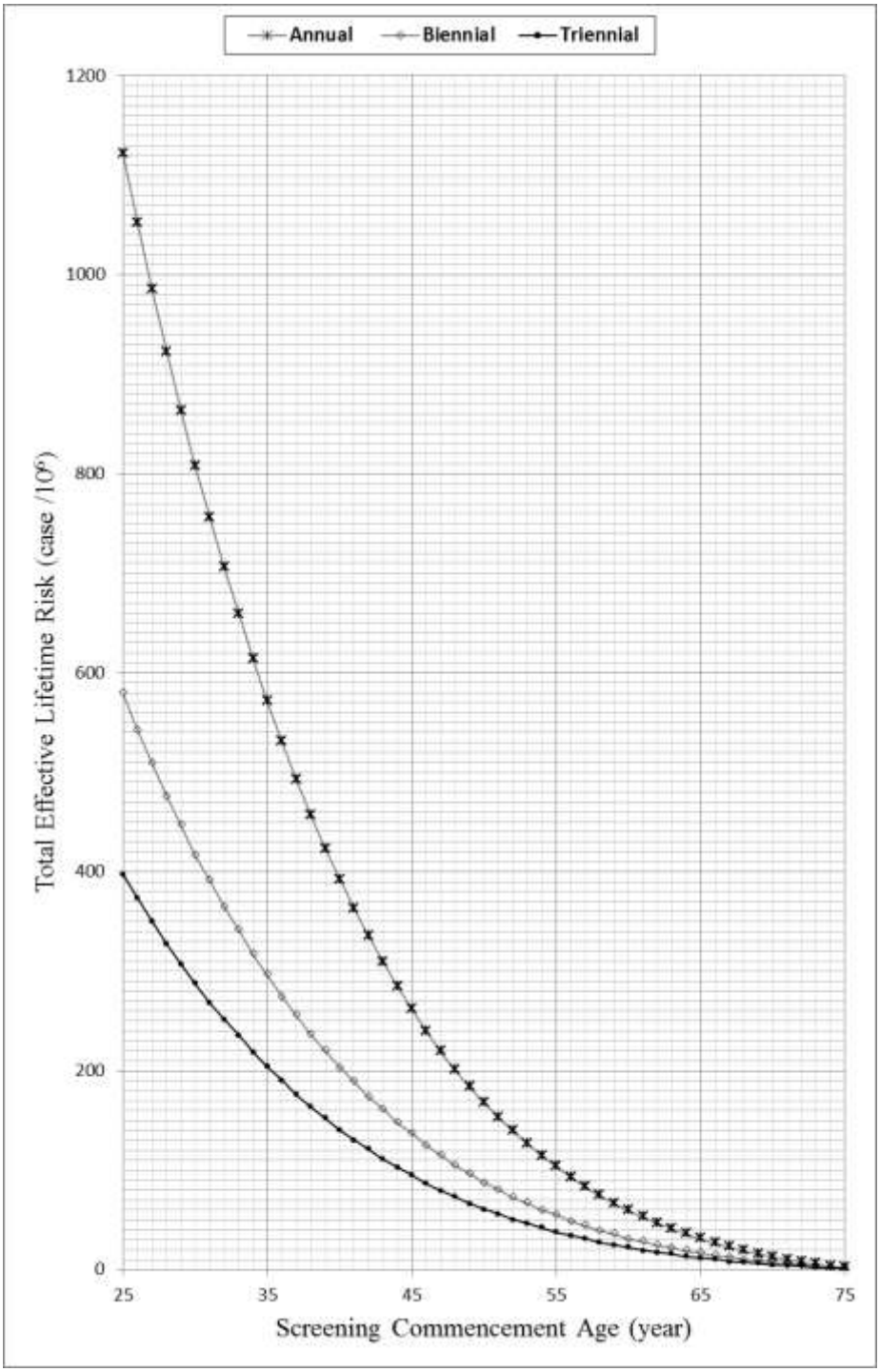

Figure (1) Represents the relationship between the total effective risk and the screening commencement age of different screening frequencies.

Using the data of sixteen FFDM machines, 450 relationship graphs were established to investigate the relationship between MGD and total effective risk of each screening scenario, for specific screening commencement ages and frequencies (Figure 2 for annual screening commence at 25 year). The relationship between MGD (μGy) and the total effective risk (case/10^6) resulted in a set of conversions factors (case/10^6/μGy) (Table 5).

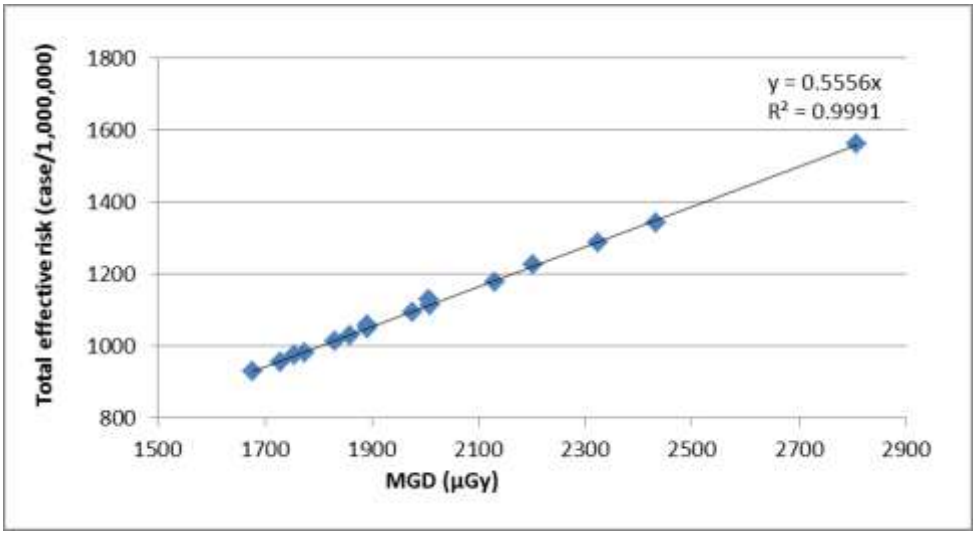

Figure (2) Relationship between MGD and total effective risk of the sixteen FFDM machines resulting from annual screening mammography commencing at 25 years old.

Table (5) Conversion factors between total effective risk of the screening programme and MGD

Commencement age (year)	Conversion factor % MGD (case/10^6/µGy)			Commencement age (year)	Conversion factor % MGD (case/10^6/µGy)		
	Annual	Biennial	Triennial		Annual	Biennial	Triennial
25	54.48	28.13	19.33	51	6.20	3.29	2.33
26	51.01	26.35	18.15	52	5.51	2.91	2.05
27	47.73	24.67	17.00	53	4.86	2.59	1.83
28	44.62	23.06	15.87	54	4.28	2.27	1.63
27	41.68	21.56	14.86	55	3.75	2.01	1.41
30	38.93	20.13	13.89	56	3.26	1.74	1.24
31	36.36	18.81	12.93	57	2.83	1.53	1.09
32	33.95	17.56	12.11	58	2.43	1.30	0.92
33	31.66	16.40	11.32	59	2.08	1.13	0.81
34	29.47	15.26	10.53	60	1.77	0.95	0.70
35	27.38	14.21	9.81	61	1.50	0.82	0.57
36	25.40	13.17	9.13	62	1.26	0.68	0.5
37	23.52	12.23	8.44	63	1.05	0.58	0.43
38	21.74	11.29	7.83	64	0.87	0.47	0.33
39	20.05	10.44	7.25	65	0.72	0.40	0.29
40	18.45	9.60	6.66	66	0.59	0.31	0.25
41	16.94	8.85	6.14	67	0.48	0.27	0.18
42	15.52	8.10	5.65	68	0.39	0.20	0.16
43	14.19	7.43	5.15	69	0.31	0.18	0.14
44	12.93	6.76	4.72	70	0.25	0.13	0.09
45	11.75	6.17	4.31	71	0.20	0.12	0.08
46	10.65	5.58	3.90	72	0.15	0.08	0.08
47	9.63	5.07	3.54	73	0.11	0.07	0.04
48	8.67	4.56	3.21	74	0.07	0.04	0.04
49	7.78	4.11	2.87	75	0.04	0.04	0.04
50	6.96	3.67	2.59				
When using this table to calculate total effective risk the commencement age and frequency of screening examinations must be selected, and the relevant conversion factor can then be multiplied by the MGD (µGy). For example, for a woman attending annual screening mammography commencing at 40 years old, she would have a total effective risk of 18.45% of her MGD (µGy); for a 2500 µGy MGD the total effective risk is 2500 X 18.45% = 461 cases/10^6							

The conversion factors listed in Table (5) enable total effective risk to be obtained for any screening programme, for any screening commencement age and frequency, whilst considering individual MGD. MGD would be derived from the initial screening mammogram. Consequently,

the graphs used in Figure (1) have been further refined to generate the graphs as illustrated in Figure (3); the modified graphs allow determination of the appropriate conversion factor.

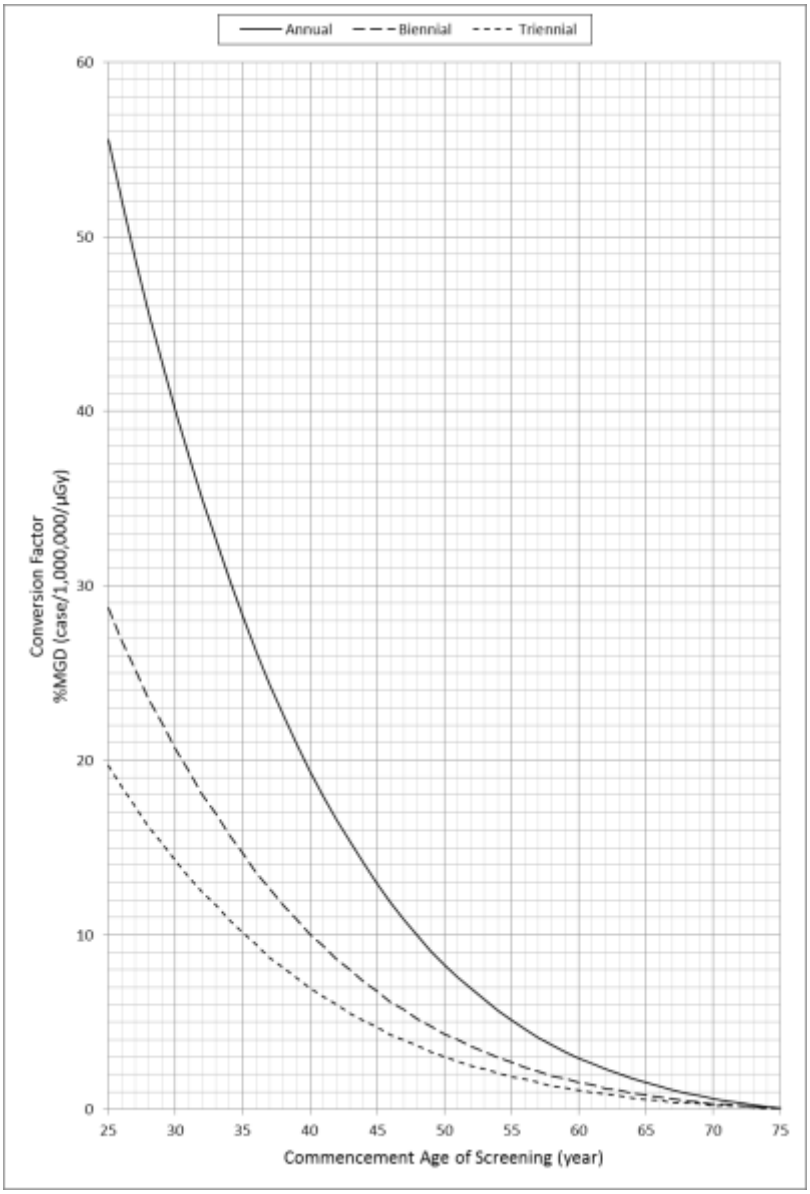

Figure (3) Relationship between total effective risk as a percentage of MGD and the screening commencement age for different screening frequencies.

Discussion

For the sixteen FFDM machines the total MGD (for both CC and MLO projections) ranged between 1.678 mGy (machine 11) and 2.806 mGy (machine 7) with a mean (95% CI) value of 2.019 (1.871 - 2.166) mGy (Table 2). These MGD values are lower than expected for a standard breast (with 53 mm thickness and 50% glandularity) because they were calculated for breasts with 29% glandularity (without the use of breast composition correction factor, c_{53} factor). This

factor is derived from Monte Carlo simulation to convert the MGD from a 29% glandularity phantom to 50% glandularity of standard breast. This was undertaken in order to make both the calculated MGD and measured organs dose consistent for 29% breast glandularity, which was simulated by a PMMA-polyethylene phantom. The standard breast composition recommended by mammographic international protocols has 50% glandularity [6, 23]. However, as reported by Yaffe et al. [24], breast glandularity used in this work (29%) represents the most common breast density. Yaffe et al. [24] found that only 5% of 2831 Canadian women studied had more than 45% breast density.

The organ doses in our work are higher than those estimated by Monte Carlo simulations in previous publications. The main reason behind this is likely to be due to the limitations inherent within mathematical phantoms used within Monte Carlo simulations [25]. For instance, the measured contralateral breast radiation dose, which was 1.419 ± 0.346 % (mean ± SD) of examined breast MGD, was approximately ~~as~~ three times that estimated by Sechopoulos et al. [11]; Sechopoulos used Monte Carlo simulation. Also, there is a lower estimated radiation dose to clavicular bone marrow (0.09 % and 0.04% of MGD for CC and MLO projections compared to 0.451 ± 0.241% MGD ; mean ± SD) and sternum bone marrow (0.49% and 0.23% MGD for CC and MLO projections compared to 0.942 ± 0.251% MGD). The measured thyroid dose in our work was approximately 10 times that estimated by Sechopoulos and Hendrick [12] which have been obtained using Monte Carlo simulation. However, ribs bone marrow and lung radiation dose was comparable with that reported by Sechopoulos et al. [11] and Leidens, Goes, and Nicolluci [13].

Despite the large variation of MGD amongst the sixteen FFDM machines (1.678 - 2.806 mGy), its contribution to effective risk is fairly constant. This can be explained by the fact that the high MGD is usually associated with high organ doses. Since the breast tissue is radio-sensitive and that it received the highest radiation dose, MGD can be seen to be directly related to radiation [mammographic] effective lifetime risk. The relationship between MGD and total effective lifetime risk for different screening scenarios is related to screening commencement age and frequency (assuming constant screening cessation age, at 75 years old). This is clearly seen in Table (5), where different relationship factors are reported for different screening scenarios. Using Figure (3), it becomes possible to obtain the total effective risk of any screening programme, for specific screening commencement ages and frequencies, whilst considering individual MGD. MGD is being derived from the initial mammogram from any FFDM machine. For a woman attended screening mammography within NHSBSP (triennial screening commences at 47 years old), her total recorded MGD (for both CC and MLO views) was 3.55 mGy (3550 µGy). The resultant total effective risk for this woman would be 142 case/10^6 (4% MGD) as derived from Figure (3).

The total effective risk data obtained in our work is consistent with previously published work. For 3.7 mGy MGD, Yaffe and Mainprize [26] found that the total risk of radiation-induced breast cancer from annual screening mammography between 40 and 49 years was 590 cases/10^6.

In our work for 2.019 mGy MGD the total effective risk of the same screening regimen was found to be 224.21 cases/10^6. Similarly for the same MGD (3.7 mGy), Hendrick [27] reported that the incidence of breast cancer resulting from annual screening between 25 - 80 years was 2040 cases/10^6. For 2.019 mGy MGD obtained in our work, 1121.36 cases/10^6 may develop cancer due to annual screening mammography between 25 -75 years. The screening mammography radiation risk from the UK recommendation was evaluated by Warren, Dance, and Young (2016). They found that it ranges between 30.7 and 61.2 cases/10^6/mGy of MGD. This is comparable to that obtained by our work; 77.79 cases/10^6 for 2.019 mGy.

Further work is required to include breast density reduction which occurs with age because this may result in a continuous reduction in woman's MGD with age. Accordingly, the extracted total effective risk from our work may be slightly exaggerated and should be considered when interpreting our data. Generated data from our work is applicable for average breast only. Other breast thicknesses and densities should be considered in future work.

Conclusion

MGD is a primary factor affecting total effective risk as it results in up to 98% of screening mammography total effective risk. The addition of MGD variation to the model established by M.Ali et al. [16] refines the model by increasing its accuracy and makes it applicable for different MGD values of different FFDM machines. Accordingly, it becomes possible to calculate total effective risk for any woman by using MGD from the initial mammogram.

References

1. Huda, W., E.L. Nickoloff, and J.M. Boone, *Overview of patient dosimetry in diagnostic radiology in the USA for the past 50 years.* Medical Physics, 2008. **35**(12): p. 5713.
2. Dance, D.R., C.L. Skinner, and G.A. Carlsson, *Breast dosimetry.* Appl Radiat Isot, 1999. **50**(1): p. 185-203.
3. Di Maria, S., et al., *TLD measurements and Monte Carlo simulations for glandular dose and scatter fraction assessment in mammography: A comparative study.* Radiation Measurements, 2011. **46**(10): p. 1103-1108.
4. Karlsson, M., et al., *Absorbed dose in mammary radiography.* Acta Radiol Ther Phys Biol, 1976. **15**(3): p. 252-8.
5. Dance, D.R., *Monte Carlo calculation of conversion factors for the estimation of mean glandular breast dose.* Pysics in medicine and biology, 1990. **35**(9): p. 1211-1219.
6. IPEM, *The commissioning and routine testing of mammographic X-ray systems*. 2005, IPEM: York.
7. Dance, D.R., et al., *Additional factors for the estimation of mean glandular breast dose using the UK mammography dosimetry protocol.* Physics in medicine and biology, 2000. **45**: p. 3225–3240.
8. Sechopoulos, I., et al., *Characterization of the homogeneous tissue mixture approximation in breast imaging dosimetry.* Med Phys, 2012. **39**(8): p. 5050-9.
9. Dance, D.R., et al., *Breast dosimetry using high-resolution voxel phantoms.* Radiat Prot Dosimetry, 2005. **114**(1-3): p. 359-63.

10. Geeraert, N., et al., *Evaluation of exposure in mammography: limitations of average glandular dose and proposal of a new quantity.* Radiat Prot Dosimetry, 2015. **165**(1-4): p. 342-5.
11. Sechopoulos , I., et al., *Radiation dose to organs and tissues from mammography: Monte Carlo and phantom study.* Radiology, 2008. **246**(2): p. 434-443.
12. Sechopoulos, I. and R.E. Hendrick, *Mammography and the risk of thyroid cancer.* AJR Am J Roentgenol, 2012. **198**(3): p. 705-7.
13. Leidens, M., E. Goes, and P. Nicolluci, *Use of Monte Carlo method to determine radiation dose to organs and tissues from mammography.* medical physics, 2013. **40**(6): p. 139.
14. Whelan, C., D. McLean, and A. Poulos, *Investigation of thyroid dose due to mammography.* Australasian radiology, 1999. **43**(3): p. 307-310.
15. Hatziioannou, K.A., et al., *Dosimetric considerations in mammography.* Eur. Radiol., 2000. **10**(7): p. 1193-1196.
16. M.Ali, R.M.K., et al., *Mathematical modelling of radiation-induced cancer risk from breast screening by mammography.* European Journal of Radiology, 2017. **96**(Supplement C): p. 98-103.
17. M.Ali, R.M.K., et al., *Effective lifetime radiation risk for a number of national mammography screening programmes.* Radiography, 2018.
18. NHSBSP, *Commissioning and routine testing of full field digital mammography systems. NHSBSP Equipment report 0604. Version 3*. 2009, NHS Cancer Screening Programmes: Sheffield.
19. CIRSTissueSimulationandPhantomTechnology, *ATOM dosimetry phantoms models 701-706*. 2012, CIRS, Inc: Virginia.
20. Tootell, A.K., K.R. Szczepura, and P. Hogg, *Optimising the number of thermoluminescent dosimeters required for the measurement of effective dose for computed tomography attenuation correction data in SPECT/CT myocardial perfusion imaging.* Radiography, 2013. **19**(1): p. 42-47.
21. Brenner, D.J., *We can do better than effective dose for estimating or comparing low-dose radiation risks.* Ann ICRP, 2012. **41**(3-4): p. 124-8.
22. NAS, N., *Health Risks from Exposure to Low Levels of Ionizing Radiation: BEIR VII – Phase 2*. 2006, National Academies Press: Washington.
23. IAEA, *Quality Assurance Programme for Digital Mammography*, in *IAEA Human Health Series*, IAEA, Editor. 2011, IAEA in Austria: Austria. p. 140.
24. Yaffe , M.J., et al., *The myth of the 50-50 breast.* Medical Physics, 2009. **36**(12): p. 5437.
25. Tootell, A., K. Szczepura, and P. Hogg, *An overview of measuring and modelling dose and risk from ionising radiation for medical exposures.* Radiography, 2014. **20**(4): p. 323-332.
26. Yaffe, M.J. and J.G. Mainprize, *Risk of radiation-induced breast cancer from mammographic screening.* Radiology, 2011. **258**(1): p. 98-105.
27. Hendrick, R.E., *Radiation doses and cancer risks from breast imaging studies.* Radiology, 2010. **257**(1): p. 246-253.